

Dynamics of high-frequency modulated waves in a nonlinear dissipative continuous bi-inductance network

S M Ngounou and F B Pelap

Citation: Chin. Phys. B, 2021, 30 (**6**): 060504. DOI: 10.1088/1674-1056/abd751
Journal homepage: http://cpb.iphy.ac.cn; http://iopscience.iop.org/cpb

What follows is a list of articles you may be interested in

Complex network perspective on modelling chaotic systems via machine learning

Tong-Feng Weng(翁同峰), Xin-Xin Cao(曹欣欣), and Hui-Jie Yang(杨会杰)
Chin. Phys. B, 2021, 30 (**6**): 060506. DOI: 10.1088/1674-1056/abd9b3

Delayed excitatory self-feedback-induced negative responses of complex neuronal bursting patterns

Ben Cao(曹奔), Huaguang Gu(古华光), and Yuye Li(李玉叶)
Chin. Phys. B, 2021, 30 (**5**): 050502. DOI: 10.1088/1674-1056/abcfa9

Design and FPGA implementation of multi-wing chaotic switched systems based on a quadratic transformation

Qing-Yu Shi(石擎宇), Xia Huang(黄霞), Fang Yuan(袁方), and Yu-Xia Li(李玉霞)
Chin. Phys. B, 2021, 30 (**2**): 020507. DOI: 10.1088/1674-1056/abd74c

A multi-directional controllable multi-scroll conservative chaos generator: Modelling, analysis, and FPGA implementation

En-Zeng Dong(董恩增), Rong-Hao Li(李荣昊), and Sheng-Zhi Du(杜升之)
Chin. Phys. B, 2021, 30 (**2**): 020505. DOI: 10.1088/1674-1056/abc239

Nonlinear continuous bi-inductance electrical line with dissipative elements: Dynamics of the low frequency modulated waves

S M Ngounou, F B Pelap
Chin. Phys. B, 2020, 29 (**4**): 040502. DOI: 10.1088/1674-1056/ab75d6

Dynamics of high-frequency modulated waves in a nonlinear dissipative continuous bi-inductance network

S M Ngounou[1,2] and F B Pelap[1,†]

[1] Unité de Recherche de Mécanique et de Modélisation des Systèmes Physiques (UR-2MSP), Faculté des Sciences, Université de Dschang, BP 69 Dschang, Cameroun

[2] Unité de Recherche de Matière Condensée d'Electronique et de Traitement du Signal (UR-MACETS), Faculté des Sciences, Université de Dschang, BP 67 Dschang, Cameroun

(Received 27 September 2020; revised manuscript received 20 December 2020; accepted manuscript online 30 December 2020)

This paper presents intensive investigation of dynamics of high frequency nonlinear modulated excitations in a damped bimodal lattice. The effects of the dissipation are considered through a linear dissipation coefficient whose evolution in terms of the carrier wave frequency is checked. There appears that the dissipation coefficient increases with the carrier wave frequency. In the linear limit and for high frequency waves, study of the asymptotic behavior of plane waves reveals the existence of two additional regions in the dispersion curve where the modulational phenomenon is observed compared to the lossless line. Based on the multiple scales method exploited in the continuum approximation using an appropriate decoupling ansatz for the voltage of the two different cells, it appears that the motion of modulated waves is described by a dissipative complex Ginzburg–Landau equation instead of a Korteweg–de Vries equation. We also show that this amplitude wave equation admits envelope and hole solitons in the high frequency mode. From basic sources, we design a programmable electronic generator of complex signals with desired characteristics, which delivers signals exploited as input waves for all our numerical simulations. These simulations are performed in the LTspice software that uses realistic components and give the results that corroborate perfectly our analytical predictions.

Keywords: dissipative bi-inductance network, high-frequency mode, continuous approximation, dissipative complex Ginzburg–Landau equation, programmable electronic generator, LT-Pspice observations

PACS: 05.45.–a, 05.45.Yv **DOI:** 10.1088/1674-1056/abd751

1. Introduction

In the recent decades, nonlinear phenomena are continuously attracting the interest of researchers in several fields of sciences.[1–6] Within these studies, behavior of discrete nonlinear systems has been of great thoughtfulness in many areas of physics. Thus, discrete nonlinear transmission lines (NLTLs) are very useful tools for investigating dynamics of waves in nonlinear dispersive media.[7,8] By their affordability and relative ease of realization, electrical transmissions lines are the simplest experimental systems for observing nonlinear phenomena and predicting new ones[9–11] such as the propagation of the solitons. Recently, Iqbal *et al.* analyzed the bifurcation with chaotic motion of oblique plane waves in an NLTL.[12] From a qualitative point of view, the origin of the soliton in the nonlinear electrical line is explained by the balance between the dispersion effect (due to the periodic positioning of the capacitor in the line) and the nonlinear linearity (due to the dependence of this capacity). In other words, these solitary waves are created when the action of the nonlinearity that leads to the compression of the packet wave is compensated for by a dispersion that tends to spread the wave. This balance between dispersion and nonlinearity induces the creation of lattice envelope solitons. Furthermore, envelope solitons can also be viewed as the result of an instability that leads to a self-induced modulation of the steady state produced by the interaction between nonlinear and dispersive effects. This phenomenon is well known as modulational instability (MI).[13–17]

In nonlinear real dispersive media, the dissipative effect coexists with both nonlinear and dispersive effects and may play a role in the wave generation and its propagation. Indeed, Yemele *et al.* examined the dynamics of modulated waves in a dissipative nonlinear LC transmission line and showed that dissipative losses in the series branch are less than those obtained in the shunt branch. They also established that wave dynamics in such a medium is governed by a type of nonlinear Schrödinger equation.[18] This amplitude equation can be used, among other things, to investigate bifurcation behaviors of oblique plane waves in the network.[19] Moreover, Abdoulkary *et al.* investigated the behavior of a modified dissipative discrete NLTL and established the generalized discrete Lange–Newell criterion for the MI phenomenon.[20] Recently, Doka proposed a dissipative electrical analog of the microtubules protein structure to show that its dynamics in the continuum limit is governed by a nonlinear perturbed Korteweg–de Vries (KdV) equation whose dark soliton solutions are determined theoretically.[21]

In spite of the above-mentioned works displaying the dissipative phenomenon in NLTLs, one could easily note that

†Corresponding author. E-mail: fbpelap@yahoo.fr

© 2021 Chinese Physical Society and IOP Publishing Ltd

there are very few investigations dealing with the nonlinear bi-inductance transmission line (NLBTL).[22–26] In this paper, we examine the impact of the dissipation on the dynamics of high frequency (HF) modulated waves in the bi-inductance transmission line using the continuous approximation. We also design the programmable electronic generator exploited to generate various complex signals used as input voltages in the NLBTL. The first part of these finding was carried out in the low-frequency (LF) mode of propagation and exhibited very interesting features.[27]

The structure of this paper is organized as follows. In Section 2, the model of dissipative NLBTL is presented and its circuit equations are derived. In Section 3, the linear dispersion law and the linear dissipative factor of the damped oscillations are determined in the low-amplitude limit. The behavior of this dissipative coefficient versus the carrier frequency is checked. In Section 4, we consider the dynamics of the modulated waves in the continuum limit. In Section 5, we use the multiple time scales method and deeply investigate the dynamics of the modulated waves in the HF mode of transmission. The amplitude wave equation for voltage motion in the dissipative NLBTL is found and the impact of the dissipation on its coefficients is investigated. We also examine the asymptotic behavior of the finite amplitude voltage in the network and appreciate the effects of the dissipative character of the system. In Section 6, we consider basic sources and design a programmable electronic generator (PEG) of complex signals (plane wave, bright soliton, dark soliton) with desired characteristics. These output signals are exploited as input wave voltages in the network for all our numerical simulations. The soliton solutions of the voltage amplitude equation are determined and their propagation observed in the network. Section 7 is reserved to discussion and concluding remarks.

2. Structural dynamics of the network

The model under consideration is a distributed NLBTL constituted of N identical unit cells made of constant inductors (L_1, L_2) and voltage-dependant capacitors $C(V)$ as depicted in Fig. 1. Hereafter, the losses due to the resistance (r_1, r_2) of the inductors as well as those induced by the conductance $g_{\rm p}$ of the capacitances are taken into account in our search. In 2013, Farota and Faye carried out experimental studies of the Fermi–Pasta–Ulam recurrence in a bimodal electrical transmission line of Fig. 1 and recovered results that corroborated the theoretical previsions.[28] Moreover, Farota *et al.* investigated experimentally the entire properties of the electrical NLBTL.[29]

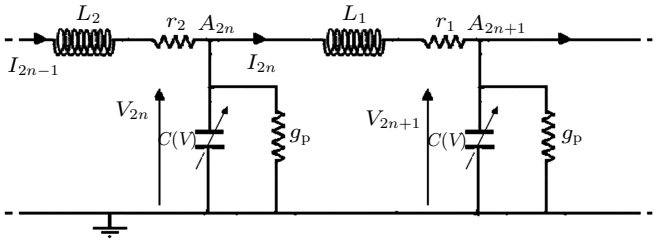


Fig. 1. Unit cell of the NLBTL. Each unit contains two real inductors (L_1, L_2) of resistances (r_1, r_2), respectively, in the series branch; two voltage dependent capacitors $C(V)$ in parallel branch with linear conductance $g_{\rm p}$.

Application of Kirchhoff's laws to the circuit of Fig. 1 leads to the following set of fundamental equations:

$$\begin{cases} L_2 \dfrac{\partial I_{2n-1}}{\partial t} + r_2 I_{2n-1} = V_{2n-1} - V_{2n}, \\ L_1 \dfrac{\partial I_{2n}}{\partial t} + r_1 I_{2n} = V_{2n} - V_{2n+1}, \\ I_{P,2n} r_{\rm p} = V_{2n}, \end{cases}$$
$$\begin{cases} I_{P,2n+1} r_{\rm p} = V_{2n+1}, \\ \dfrac{\partial Q_{2n}}{\partial t} = I_{2n-1} - I_{2n} - I_{P,2n}, \\ \dfrac{\partial Q_{2n+1}}{\partial t} = I_{2n} - I_{2n+1} - I_{P,2n+1}. \end{cases} \tag{1}$$

In Eq. (1), the subscript t denotes the time differentiation, I_{2n} represents the current passing through the $2n$-th linear inductor with constant inductance L_1, and $Q_{2n}(t)$ designates the charge stored in the $2n$-th nonlinear capacitor $C(V_{2n}) = {\rm d}Q_{2n}/{\rm d}V_{2n}$ biased by the dc bias voltage V_0. The quantities $I_{P,2n}$ and $I_{P,2n+1}$ define the current flowing in the conductance $g_{\rm p}$ in the cells of rang $2n$ and $2n+1$, respectively. For low voltages taken around V_0, the dependence $Q_{2n}(V_{2n})$ may be approximated by[26] $Q_{2n}(V_{2n}) \approx C_0 \left(V_{2n} - \alpha V_{2n}^2\right)$, where α represents the nonlinear parameter and $C_0 = C(V_0)$ defines the characteristic capacitance. For $V_0 = 1.5$ V, we obtain $\alpha = 0.159$ V^{-1} and $C_0 = 540$ pF.[24] To continue, the explicit form of $Q_{2n}(V_{2n})$ defined above is exploited to eliminate the current in the circuit Eq. (1) and express them in terms of the voltages $V_n(t)$ and $W_n(t)$ as follows:

$$\begin{aligned} &\left(V_n - \alpha V_n^2\right)_{tt} + \mu_{r1}\left(V_n - \alpha V_n^2\right)_t + \gamma_{\rm rp} V_{n,t} \\ &= Y_2 (W_n - V_n) - Y_1 (V_n - W_{n+1}) - \mu_{r1}\gamma_{\rm rp} V_n, \\ &\left(W_{n+1} - \alpha W_{n+1}^2\right)_{tt} + \mu_{r2}\left(W_{n+1} - \alpha W_{n+1}^2\right)_t + \gamma_{\rm rp} W_{n+1,t} \\ &= Y_1 (V_n - W_{n+1}) - Y_2 (W_{n+1} - V_{n+1}) - \mu_{r2}\gamma_{\rm rp} W_{n+1}, \end{aligned} \tag{2}$$

where $V_n(t)$ denotes the voltage of the even cells (V_{2n}) with inductance L_2, and $W_n(t)$ represents the voltage of the odd cells (V_{2n-1}) with inductance L_1. In deriving Eq. (2), we set $Y_1 = 1/L_1C_0$, $Y_2 = 1/L_2C_0$, $\mu_{r1} = r_1/L_1$, $\mu_{r2} = r_2/L_2$ and $\gamma_{\rm rp} = g_{\rm p}/C_0$ with $g_{\rm p} = 1/r_{\rm p}$. Expressions (2) comprise a set of $2N$ coupled nonlinear difference-differential equations to be solved in the upcoming sections. Let us remind that $n = 1, 2, \ldots, N$, where N is the number of cells considered in the network.

3. Dynamics of the linear waves

In this section, we consider the linear domain and seek the behavior of waves in the lattice. Hence, the differential capacitance $C(V)$ is constant and the charge stored in the $2n$-th capacitor is reduced to $Q_{2n}(V_n) \approx C_0(V_n)$. Thus, the basic Eqs. (2) that characterize the network become

$$\begin{aligned} &(V_n)_{tt} + \mu_{r1}(V_n)_t + \gamma_{\rm rp} V_{n,t} \\ &= Y_2(W_n - V_n) - Y_1(V_n - W_{n+1}) - \mu_{r1}\gamma_{\rm rp} V_n, \\ &(W_{n+1})_{tt} + \mu_{r2}(W_{n+1})_t + \gamma_{\rm rp} W_{n+1,t} \\ &= Y_1(V_n - W_{n+1}) - Y_2(W_{n+1} - V_{n+1}) - \mu_{r2}\gamma_{\rm rp} W_{n+1}. \end{aligned} \tag{3}$$

At this level, we intend to examine the behavior of travelling plane waves in this system. Since the network possesses non-neglected sources of dissipation, we assume that the excitation has a complex wave number of the form $k = k_{\rm p} + {\rm i}\chi$, in which $k_{\rm p}$ and χ are, respectively, the wave number of the carrier and its linear dissipation coefficient, with the quantity $i = \sqrt{-1}$ being a complex number. Then the linear wave solutions to Eq. (3) are taken as follows:

$$U_n(t) = B_2 \exp(-2n\chi) \cdot \exp\left[{\rm i}(2nk_{\rm p} - \omega t)\right] + {\rm c.c.}, \tag{4a}$$

$$W_n(t) = B_1 \exp[-(2n-1)\chi] \cdot \exp\left\{{\rm i}[(2n-1)k_{\rm p} - \omega t]\right\} + {\rm c.c.}, \tag{4b}$$

where ω is the frequency of the carrier waves of amplitudes B_1 and B_2; c.c. means the complex conjugate of the preceding term since the signal voltage is real. The first (resp. the second) expression in (4) defines waves that evolve only in cells with linear inductance L_2 (resp. L_1). Substituting relations (4) into Eqs. (3) and retaining only linear terms lead to a linear homogeneous system for B_1 and B_2:

$$aB_1 + bB_2 = 0, \quad dB_1 + cB_2 = 0, \tag{5}$$

with $a = \omega^2 + \mu_{r2}{\rm i}\omega + \gamma_{\rm rp}{\rm i}\omega - Y_{12} - \mu_{r2}\gamma_{\rm rp}$, $b = Y_1 {\rm e}^{\chi} {\rm e}^{-{\rm i}k_{\rm p}} + Y_2 {\rm e}^{-\chi} {\rm e}^{{\rm i}k_{\rm p}}$, $Y_{12} = Y_1 + Y_2$, $c = \omega^2 + \mu_{r1}{\rm i}\omega + \gamma_{\rm rp}{\rm i}\omega - Y_{12} - \mu_{r1}\gamma_{\rm rp}$ and $d = Y_2 {\rm e}^{\chi} {\rm e}^{-{\rm i}k_{\rm p}} + Y_1 {\rm e}^{-\chi} {\rm e}^{{\rm i}k_{\rm p}}$.

The condition for the existence of nontrivial solutions to Eqs. (5) gives

$$\begin{aligned} &\left\{\cos(2k_{\rm p})\left[\exp(2\chi) + \exp(-2\chi)\right] + \frac{F_0}{D_0}\right\} \\ &+ {\rm i}\left\{\sin(2k_{\rm p})\left[\exp(-2\chi) - \exp(2\chi)\right] + \frac{G_0}{D_0}\right\} = 0. \end{aligned} \tag{6}$$

Due to the uniqueness of the development (6), its real part acts as the linear dispersion relation between $k_{\rm p}$ and ω, i.e.,

$$\cos(2k_{\rm p}) = -\frac{F_0}{2D_0 ch(2\chi)} \tag{7}$$

and its imaginary part may act as the linear dissipation equation for χ and yields

$$\chi = 2^{-1}\log\left(\vartheta + \sqrt{\vartheta^2 - 1}\right). \tag{8}$$

In the previous Eqs. (6)–(8), we have set

$$\vartheta = \sqrt{1 + \frac{\eta_0^2 + \phi_0^2 - 1 + \left[(\eta_0^2 + \phi_0^2 + 1)^2 - 4\eta_0^2\right]^{1/2}}{2}},$$

$$\eta_0 = -\frac{F_0}{2D_0}, \quad \phi_0 = \frac{G_0}{2D_0},$$

with $D_0 = -Y_1 Y_2$,

$$\begin{aligned} G_0 &= \omega^3\left[\mu_{r1} + \mu_{r2} + 2\gamma_{\rm rp}\right] \\ &\quad - \omega[2\mu_{r1}\mu_{r2}\gamma_{\rm rp} + \mu_{r1}\gamma_{\rm rp}^2 + \mu_{r2}\gamma_{\rm rp}^2 \\ &\quad + \mu_{r1}Y_{12} + \mu_{r2}Y_{12} + 2\gamma_{\rm rp}Y_{12}], \\ F_0 &= \omega^4 - \omega^2\left[\mu_{r1}\mu_{r2} + 2\mu_{r1}\gamma_{\rm rp} + 2\mu_{r2}\gamma_{\rm rp} + \gamma_{\rm rp}^2 + 2Y_{12}\right] \\ &\quad + \mu_{r1}\mu_{r2}\gamma_{\rm rp}^2 + \mu_{r1}\gamma_{\rm rp}Y_{12} + \mu_{r2}\gamma_{\rm rp}Y_{12} \\ &\quad - Y_1^2 - Y_2^2 + Y_{12}^2. \end{aligned}$$

In the absence of dissipation (i.e., $\mu_{r1} = \mu_{r2} = \mu_{\rm rp} = 0$ then $\vartheta = 1$ and $\chi = 0$), the linear spectrum (7) is reduced to the well-known dispersion relation of the typical cut-band filter of the lossless NLBTL:[22,24]

$$\begin{aligned} \omega^2 &= \frac{1}{C_0}\left\{\left(\frac{1}{L_1} + \frac{1}{L_2}\right)\right. \\ &\quad \left. \pm\sqrt{\left(\frac{1}{L_1} + \frac{1}{L_2}\right)^2 - \frac{4}{L_1 L_2}\sin^2(k_{\rm p})}\right\}, \end{aligned} \tag{9}$$

wherein the signs $+$ and $-$ refer, respectively, to the LF and HF modes of transmission. In the following, we focus our attention on the nonlinear behavior of the network. This plot of Fig. 2 showing the evolution of the frequency in terms of the wave number confirms the existence of these two modes of transmission in our damped lattice: the LF mode for frequencies $f \in [0,\ 1.835\ {\rm MHz}]$ and the HF mode for frequencies belonging to the range $[2.587\ {\rm MHz},\ 3.174{\rm MHz}]$. Figure 2 exhibits the frequency bandwidth of the line of Fig. 1 for given system parameters. This curve also allows noting the forbidden frequency region for which the network cannot support wave transmission for the same parameters. To close this section, we seek the behavior of the linear dissipation coefficient χ in terms of the carrier frequency chosen in the HF mode of propagation. It appears from the plots of Fig. 3 that the dissipation coefficient grows with the growth of the carrier frequency showing that low values of the dissipation coefficient are indicated during the signal voltage transmission in the HF mode. In the upcoming sections, we examine its impact on the other system parameters.

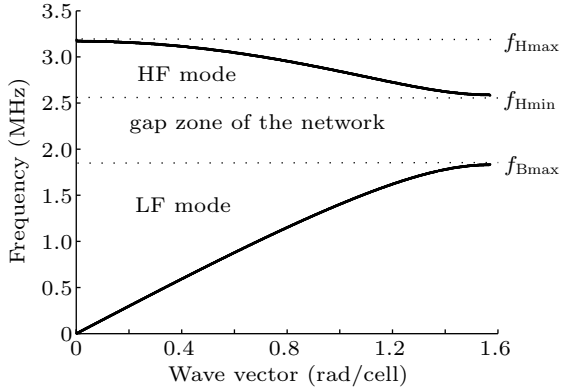


Fig. 2. Dispersion curves versus the wave number of the carrier wave for the line parameters $L_1 = 28$ μH, $L_2 = 14$ μH, $V_0 = 1.5$ V, $C_0 = 540$ pF, $r_1 = 10^{-3}$ Ω, $r_2 = 0.5 \times 10^{-3}$ Ω, $g_{\mathrm{p}} = 10^{-7}$ S and $\alpha = 0,159$ V^{-1}. This curve shows the existence of two different modes of transmission in the network: the LF mode ($f \in [0, 1835$ kHz$]$) and the HF mode ($f \in [2587$ kHz, 3174 kHz$]$) separated by a gap zone ($f \in [1835$ kHz, 2587 kHz$]$).

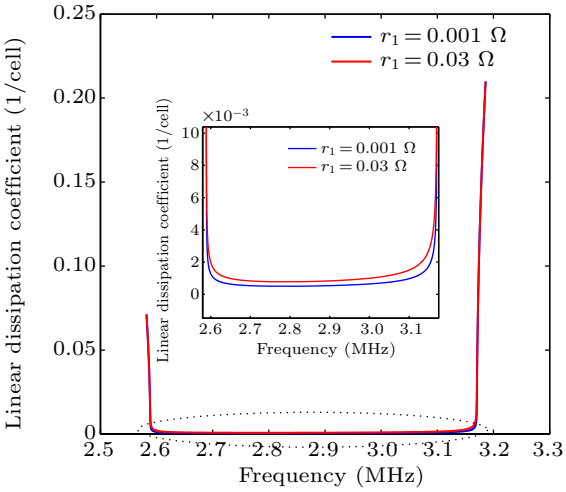


Fig. 3. Variation of the linear dissipation coefficient $\chi(\mathrm{cell}^{-1})$ as a function of the frequency f (MHz) chosen in the HF mode for the line parameters of Fig. 2 and several values of r_1.

4. Dynamics of modulated waves in the continuum limit

Here, we describe the general mathematical approach used to investigate modulated waves transmission in the NLBTL considering the continuum approximation (CA). To understand our motivation, we start by reminding that Kofane *et al.*[22] considered the CA and established that the behavior of nonlinear excitations in a lossless NLBTL is governed by a KdV-type equation that admits pulse soliton solutions. Then, Pelap *et al.*[24] showed that the dynamics of modulated waves in the same network while considering the semi-discrete approximation is described by a complex Ginzburg–Landau (CGL) equation. These results (P_i, $Q_i \neq 0$) show that the bi-inductance line seems to generate damped dispersion and nonlinearity. Trying to understand how this phenomenon occurs, we plan to use the continuous approximation and deeply look for the behavior of modulated waves in the dissipative NLBTL using the analytical techniques developed for diatomic chains.[30] Therefore, we apply the CA for the voltage of each inductance separately (i.e., if we put $x = 2n$) and obtain the upcoming expansions for $U_{n\pm1}$ and $W_{n\pm1}$ in terms of the Taylor series

$$\begin{aligned} V_{n\pm1} &= V \pm 2\varepsilon\frac{\partial V}{\partial x} + 2\varepsilon^2\frac{\partial^2 V}{\partial x^2} \pm \frac{4}{3}\varepsilon^3\frac{\partial^3 V}{\partial x^3} + \frac{2}{3}\varepsilon^4\frac{\partial^4 V}{\partial x^4} \\ &\quad \pm \frac{4}{15}\varepsilon^5\frac{\partial^5 V}{\partial x^5} + \frac{4}{45}\varepsilon^6\frac{\partial^6 V}{\partial x^6} + \mathrm{O}\left(\varepsilon^7\right), \end{aligned} \tag{10a}$$

$$\begin{aligned} W_{n\pm1} &= W \pm 2\varepsilon\frac{\partial W}{\partial x} + 2\varepsilon^2\frac{\partial^2 W}{\partial x^2} \pm \frac{4}{3}\varepsilon^3\frac{\partial^3 W}{\partial x^3} + \frac{2}{3}\varepsilon^4\frac{\partial^4 W}{\partial x^4} \\ &\quad + \frac{4}{15}\varepsilon^5\frac{\partial^5 W}{\partial x^5} + \frac{4}{45}\varepsilon^6\frac{\partial^6 W}{\partial x^6} + \mathrm{O}\left(\varepsilon^7\right). \end{aligned} \tag{10b}$$

In these relations, ε is a small scaling parameter such that $\partial/\partial t \sim \mathrm{O}(\varepsilon)$, $\partial/\partial x \sim \mathrm{O}(\varepsilon)$, and 2ε measures the distance between two consecutive identical linear inductances. This also means that we are only interested in waves varying slowly in time and space. Exploitation of the relations (10) helps in transforming Eq. (3) in two partial differential equations for $V(x,t)$ and $W(x,t)$:

$$\begin{aligned} &(V - \alpha V^2)_{tt} + \mu_{r2}(V - \alpha V^2)_t + \gamma_{\mathrm{rp}} V_t \\ &= -Y_2(V - W) + Y_1(W_{n+1} - V) - \mu_{r2}\gamma_{\mathrm{rp}} V, \end{aligned} \tag{11a}$$

$$\begin{aligned} &(W - \alpha W^2)_{tt} + \mu_{r1}(W - \alpha W^2)_t + \gamma_{\mathrm{rp}} W_t \\ &= Y_2(V - W) - Y_1(W - V_{n+1}) - \mu_{r1}\gamma_{\mathrm{rp}} W. \end{aligned} \tag{11b}$$

Because Eqs. (11) are still coupled, we make use of the following decoupling ansatz[30] obtained by expanding $W(x,t)$ in terms of $V(x,t)$ and its derivatives:

$$\begin{aligned} W &= \sigma\Big[V + \varepsilon b_1 V_x + \frac{1}{2}\varepsilon^2 b_2 V_{2x} + \frac{1}{6}\varepsilon^3 b_3 V_{3x} + \frac{1}{24}\varepsilon^4 b_4 V_{4x} \\ &\quad + \frac{1}{120}\varepsilon^5 b_5 V_{5x} + \frac{1}{720}\varepsilon^6 b_6 V_{6x} + \mathrm{O}\left(\varepsilon^7\right)\Big], \end{aligned} \tag{12}$$

where σ and b_j $(j = 1, \ldots, 6)$ are parameters to be determined. Substitution of expression (12) into Eqs. (11) gives:

$$\begin{aligned} &\varepsilon^2(V - \alpha V^2)_{tt} + \varepsilon\mu_{r2}(V - \alpha V^2)_t + \varepsilon\gamma_{\mathrm{rp}} V_t \\ &= AV + \varepsilon B V_x + \varepsilon^2 C V_{2x} \\ &\quad + \varepsilon^3 D V_{3x} + \varepsilon^4 E V_{4x} + F V_{5x} + G V_{6x}, \end{aligned} \tag{13a}$$

$$\begin{aligned} &\varepsilon^2(W - \alpha W^2)_{tt} + \varepsilon\mu_{r1}(W - \alpha W^2)_t + \varepsilon\gamma_{\mathrm{rp}} W_t \\ &= A'V + \varepsilon B' V_x + \varepsilon^2 C' V_{2x} \\ &\quad + \varepsilon^3 D' V_{3x} + \varepsilon^4 E' V_{4x} + F' V_{5x} + G' V_{6x}. \end{aligned} \tag{13b}$$

The parameters of Eqs. (13) are defined in the Appendix. The compatibility of the expressions (13a) and (13b) means that the two equations for $V(x,t)$ are equivalent. Then, we can derive the following equivalences:

$$A = A', \tag{14a}$$

$$B = B', \tag{14b}$$

$$C = C', \tag{14c}$$

$$D = D', \tag{14d}$$

$$E = E', \tag{14e}$$
$$F = F', \tag{14f}$$
$$G = G'. \tag{14g}$$

The resolution of Eqs. (14) helps in completing information related to the system under study. Indeed, from Eq. (14a), we obtain two values of σ that are $\sigma = \pm 1$. The value $\sigma = +1$ leads to the LF mode of propagation where the voltages V and W in one cell are in phase whereas the value $\sigma = -1$ deals with the HF mode of transmission where the two voltages are opposite in phase. Hereafter, we investigate the dynamics of the system in the HF mode of transmission.

5. Dynamics of the high-frequency excitations

5.1. Amplitude equation

Here, the dynamics of modulated waves along the dissipative NLBTL of Fig. 1 in the HF mode of transmission that deals with $\sigma = -1$ is checked. For this value of σ, we solve Eqs. (14b)–(14g) by keeping terms up to $O(\varepsilon^7)$ and obtain respectively:

$$\begin{aligned}
&b_1 = 2L/L_1, \quad b_2 = 4L^2/L_1^2 = b_1^2,\\
&b_3 = 3b_1^3 - 6b_1^2 + 4b_1, \quad b_4 = 9b_1^4 - 24b_1^3 + 16b_1^2,\\
&b_5 = 45b_1^5 - 180b_1^4 + 240b_1^3 - 120b_1^2 + 16b_1,\\
&b_6 = b_{61}/b_{62},
\end{aligned} \tag{15}$$

with $b_{61} = 128Y_1\left(225Y_1^5 - 540Y_1^4Y_{12} + 450Y_1^3Y_{12}^2 - 150Y_1^2Y_{12}^3 + 16Y_1Y_{12}^4\right)$ and $b_{62} = Y_{12}^5\left(Y_{12}\mu_{r2}\gamma_{rp} - \mu_{r1}\gamma_{rp} - 2Y_{12}\right)$.

The substitution of expresses (15) into Eq. (12) helps to obtain the explicit form of the decoupling ansatz W, that is,

$$\begin{aligned}
W \;=\; & V + \varepsilon b_1 V_x + \frac{1}{2}\varepsilon^2 b_1^2 V_{2x} + \frac{1}{6}\varepsilon^3\left(3b_1^3 - 6b_1^2 + 4b_1\right)V_{3x} + \frac{1}{24}\varepsilon^4\left(9b_1^4 - 24b_1^3 + 16b_1^2\right)V_{4x}\\
& + \frac{1}{120}\varepsilon^5\left(45b_1^5 - 180b_1^4 + 240b_1^3 - 120b_1^2 + 16b_1\right)V_{5x}\\
& + \frac{1}{720}\varepsilon^6\left(\frac{128Y_1(225Y_1^5 - 540Y_1^4Y_{12} + 450Y_1^3Y_{12}^2 - 150Y_1^2Y_{12}^3 + 16Y_1Y_{12}^4)}{Y_{12}^5(Y_{12}\mu_{r2}\gamma_{rp} - \mu_{r1}I_{rp} - 2Y_{12})}\right)V_{6x} + O(\varepsilon^7).
\end{aligned}$$

Substitution of expresses (15) into Eqs. (14) yields a single equation for $U(x,t)$ (or $W(x,t)$) which includes the influence of cells of the other rank (odd or even) owing to the starting considerations, namely,

$$\begin{aligned}
&U_{tt} - \alpha\left(U^2\right)_{tt} + \alpha\mu_{r2}U_t^2\\
&= A''U + C''U_{2x} + E''U_{4x} + G''U_{6x} + H''U_t,
\end{aligned} \tag{16}$$

where

$$\begin{aligned}
&A'' = -\mu_{r2}\gamma_{rp} - 2\mu_{12}, \quad C'' = -2Y_1 + 2Y_1^2/Y_{12},\\
&B'' = D'' = F'' = 0, \quad H'' = -\mu_{r2} - \gamma_{rp},\\
&E'' = 2Y_1\left(3Y_1^3 - 6Y_1^2Y_{12} + 4Y_{12}Y_1^2 - Y_{12}^3\right)/3Y_{12}^3,\\
&G'' = 4Y_1(\phi + \eta + \mu)\left[45Y_{12}^5(Y_{12}\mu_{r2}\gamma_{rp} + 2Y_{12}^2 - \mu_{r1}\gamma_{rp})\right]^{-1},
\end{aligned}$$

with

$$\begin{aligned}
\phi \;=\; & Y_1(270Y_1^5Y_{12}\mu_{r2}\gamma_{rp} - 675Y_1^4Y_{12}^2\mu_{r2}\gamma_{rp} + 600Y_1^3Y_{12}^3\mu_{r2}\gamma_{rp}\\
& - 225Y_1^2Y_{12}^4\mu_{r2}\gamma_{rp} + 32Y_1Y_{12}^5\mu_{r2}\gamma_{rp} - Y_t^6\mu_{r2}\gamma_{rp},\\
\eta \;=\; & 540Y_1^5Y_{12}^2 - 270Y_1^5\mu_{r1}\gamma_{rp} - 1350Y_1^4Y_{12}^3 + 675Y_1^4Y_{12}\mu_{r1}\gamma_{rp}\\
& + 1200Y_1^3Y_{12}^4 - 600Y_1^3Y_{12}^2\mu_{r1}\gamma_{rp} - 450Y_1^2Y_{12}^5,\\
\mu \;=\; & 225Y_1^2Y_{12}^3\mu_{r1}\gamma_{rp} + 64Y_1Y_{12}^6 - 32Y_1Y_{12}^4 + 2Y_{12}^7\\
& + Y_{12}^5\mu_{r1}\gamma_{rp} - 450Y_1^5Y_{12} + 1080Y_1^4Y_{12}^2 - 900Y_1^3Y_{12}^3\\
& + 300Y_1^2Y_{12}^4 - 32Y_1Y_{12}^5.
\end{aligned}$$

Expression (16) represents a damped Boussinesq-type equation for the voltage $U(x,t)$[31] wherein the quantity C'' designates the velocity of the linear non-dispersive waves and A'', E'', G'', H'' are positive constants. In the small amplitude limit, Eq. (16) can be reduced to the universal KdV equation by introducing a suitable transformation. Hereafter, instead of searching the pulse solution characteristic of the KdV systems as it was done by Kofane *et al.*,[22] we look for the modulated wave solutions of Eq. (16). Following this aim, we call the multiple scales method where x and t are scaled into independent variables $x_0, x_1, \ldots, x_n$ and $t_0, t_1, \ldots, t_n$, respectively, with $x_n = \varepsilon^n x$, $t_n = \varepsilon^n t$. Therefore, Eq. (16) is transformed up to the second harmonic generation. For convenience, we introduce $U \to \varepsilon U_1$ and replace x_0, x_1 and t_0, t_1, respectively, by x, X and t, T. Hence, Eq. (16) can be written as

$$\begin{aligned}
&U_{1,tt} + 2\varepsilon U_{1,tT} + \varepsilon^2 U_{1,TT}\\
&- \alpha\left\{U_{1,tt}^2 + 2\varepsilon\left(U_1^2\right)_{tT} + \varepsilon^2\left(U_1^2\right)_{TT}\right\}\\
&+ \alpha\mu_{r2}\left\{\left(U_1^2\right)_t + \varepsilon\left(U_1^2\right)_T\right\}\\
&= A''U_1 + C''\left\{U_{1,2x} + 2\varepsilon U_{1,xX} + \varepsilon^2 U_{1,XX}\right\}\\
&+ E''\left\{U_{1,4x} + 4\varepsilon U_{1,3xX} + 6\varepsilon^2 U_{1,2x2X} + 4\varepsilon^3 U_{1,x3X} + \varepsilon^4 U_{1,4X}\right\}\\
&+ G''\left\{U_{1,6x} + 6\varepsilon U_{1,5xX} + 15\varepsilon^2 U_{1,4x2X} + 20\varepsilon^3 U_{1,3x3X}\right.\\
&\left. + 15\varepsilon^4 U_{1,2x4X} + 6\varepsilon^5 U_{1,x5X} + \varepsilon^6 U_{1,6X}\right\} + H''U_{1,t}.
\end{aligned} \tag{17}$$

The modulated wave solutions to Eq. (17) are chosen in the general form[24]

$$U_1 \;=\; \varepsilon U_{11}(X,T)\exp\left[i(kx - \Omega t)\right] + \text{c.c.} + \varepsilon^2 U_{20}(X,T)$$

$$+\varepsilon^2 U_{22}(X,T)\exp[2\mathrm{i}(kx-\Omega t)]+\text{c.c.}, \quad (18)$$

where c.c. designates the complex conjugate of the preceding term, k represents the complex wave number ($k=k_\mathrm{p}+\mathrm{i}\chi$) of the carrier and Ω defines its angular frequency, which satisfy the following complex relation:

$$\begin{aligned}&\left[\Omega^2+A''+C''(\chi^2-k_\mathrm{p}^2)+E''(\chi^4-6\chi^2k_\mathrm{p}^2+kp^4)\right.\\&\left.+G''(\chi^6-15\chi^4k_\mathrm{p}^2+15\chi^2k_\mathrm{p}^4-k_\mathrm{p}^6)\right]\\&+\mathrm{i}\left[-2C''k_\mathrm{p}\chi+E''(-4\chi^3k_\mathrm{p}+4\chi k_\mathrm{p}^3)\right.\\&\left.+G''(-6\chi^5k_\mathrm{p}+20\chi^3k_\mathrm{p}^3-6\chi kp^5)-H''\Omega\right]=0. \quad (19)\end{aligned}$$

Resolution of Eq. (19) leads, respectively, to the dispersion law (7) and the linear dissipative coefficient (8) for the HF mode of transmission. At this level, the procedure is to substitute Eq. (18) into Eq. (17) and apply the secular conditions to the resulting equation. Therefore, the terms proportional to $\varepsilon^2\mathrm{e}^{2\mathrm{i}(kx-\omega t)}$ and $\varepsilon^4\mathrm{e}^{0\mathrm{i}(kx-\omega t)}$ permit to determine, respectively, the voltages

$$U_{22}=A_{11}U_{11}^2 \quad \text{and} \quad U_{20}=A_{12}|U_{11}|^2 \quad (20)$$

with

$$\begin{aligned}A_{11}&=[4\alpha\Omega-\mathrm{i}2\alpha\mu_{r2}\Omega]/D_1,\\A_{12}&=2\alpha V_\mathrm{g}^2\exp(-2\chi x)/\left(V_\mathrm{g}^2-C\right),\\D_1&=4\Omega+A''+4C''\left(\mathrm{i}k_\mathrm{p}-\chi\right)^2\\&\quad+16E''\left(\mathrm{i}k_\mathrm{p}-\chi\right)^4+64G''\left(\mathrm{i}k_\mathrm{p}-\chi\right)^6-2\mathrm{i}\Omega H''.\end{aligned}$$

Hereafter, we collect information to the third order terms (i.e., $\mathrm{O}(\varepsilon^3)$) of the first harmonic and set $z=X-V_\mathrm{g}T$ and $\tau=\varepsilon T$. While exploiting these transformations together with the voltage expressions (20), one obtains that the evolution of a packet wave in the HF mode of the continuous dissipative bi-inductance line is described by the following dissipative CGL equation:

$$\mathrm{i}\frac{\partial V_{11}}{\partial\tau}+P_1\frac{\partial^2V_{11}}{\partial z^2}+Q_1|V_{11}|^2V_{11}=\mathrm{i}J_1V_{11}. \quad (21)$$

In this equation, the coefficient J_1 materializes the dissipation produces in the network due to the imperfection of the differential capacitance $C(V)$ justified here by the presence of the conductance g_p in the circuit. Equation (21) is well known as a basic model to describe phase transitions and wave propagation in various systems.[22,32–34] Within Eq. (21), the dispersion coefficient $P_1P_{1\mathrm{r}}+\mathrm{i}P_{1\mathrm{i}}$ and the nonlinear coefficient $Q_1=Q_{1\mathrm{r}}+\mathrm{i}Q_{1\mathrm{i}}$ are, respectively, defined by

$$\begin{aligned}P_1&=\frac{1}{2\Omega}\left\{-V_{gf}^2-\beta_3^2-2\mathrm{i}\beta_3V_{gf}+C''\right.\\&\quad\left.+6E''\left(\mathrm{i}k_\mathrm{p}-\chi\right)^2+15G''\left(\mathrm{i}k_\mathrm{p}-\chi\right)^4\right\}, \quad (22a)\\Q_1&=\mathrm{i}\alpha\Omega\mu_{r2}A_{12}-\alpha\Omega\left[A_{11}\exp(-2\chi x)+A_{12}\right], \quad (22b)\end{aligned}$$

where

$$\beta_3=\frac{K_2H_{14}+K_3H_{15}}{16\beta_4\left[H_{16}+\sqrt{K_2^2+K_3^2}\right]}$$

with the other quantities defined as follows:

$$\begin{aligned}K_2&=-4G''\left(\chi^6-15\chi^4k_\mathrm{p}^2+15\chi^2k_\mathrm{p}^4-k_\mathrm{p}^6\right)\\&\quad-4E''\left(\chi^4-6\chi^2k_\mathrm{p}^2+k_\mathrm{p}^4\right)\\&\quad-4C''\left(\chi^2-k_\mathrm{p}^2\right)-H''^2-4A'',\\K_3&=8G''\left(3\chi^5k_\mathrm{p}-10\chi^3k_\mathrm{p}^3+3\chi k_\mathrm{p}^5\right)\\&\quad+16E''\left(\chi^3k_\mathrm{p}-\chi k_\mathrm{p}^3\right)+8C''\chi k_\mathrm{p},\\H_{14}&=-24G''\left(\chi^5-10\chi^3k_\mathrm{p}^2+5\chi^3k_\mathrm{p}^2\right)\\&\quad-16E''\left(\chi^3-3\chi k_\mathrm{p}^2\right)-8C''\chi,\\H_{15}&=24G''\left(5\chi^4k_\mathrm{p}-10\chi^2k_\mathrm{p}^3+k_\mathrm{p}^5\right)\\&\quad+16E''\left(4\chi^2k_\mathrm{p}-k_\mathrm{p}^3\right)+8C''k_\mathrm{p},\\H_{16}&=-2H_{14},\\\beta_4&=\frac{1}{2}H''+\frac{1}{4}\left(2\sqrt{K_2^2+K_3^2}-2K_2\right)^{\frac{1}{2}}.\end{aligned}$$

The analytical expressions of $P_{1\mathrm{r}}$, $P_{1\mathrm{i}}$, $Q_{1\mathrm{r}}$ and $Q_{1\mathrm{i}}$ were not reachable. However, we separate P_1 (resp. Q_1) into real and imaginary parts during numerical simulations. We also check the effects of the dissipation on the dispersive and nonlinear coefficients of the CGL equations (Figs. 4 and 5).

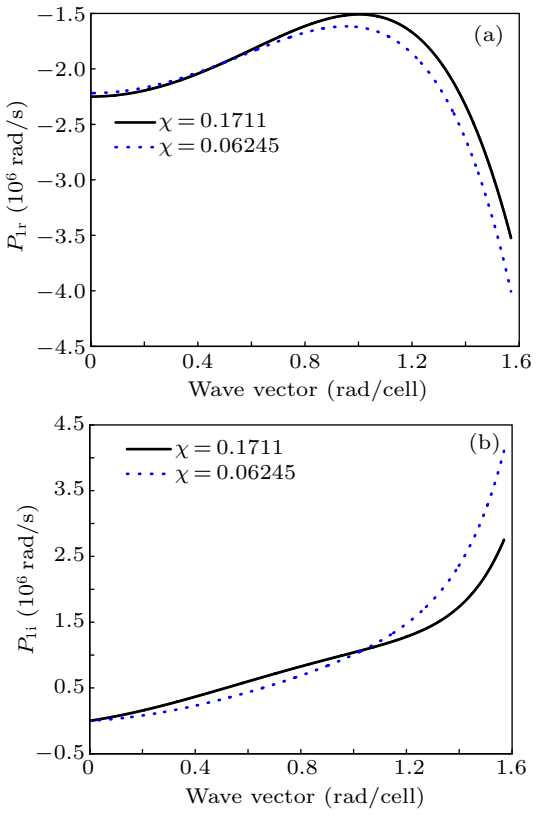


Fig. 4. Effects of the dissipation on the dispersion coefficient ($P_{1\mathrm{r}}$, $P_{1\mathrm{i}}$) as a function of the wave number for the line parameters of Fig. 2 and several values of χ.

These plots show the behavior of the coefficients of the CGL equation as a function of the wave number k_p of the carrier for several values of the linear dissipation rate χ. It appears that these coefficients (P_{1r}, P_{1i}, Q_{1r}, Q_{1i}) are non nulls and their profile changes with the growth of χ.

Concretely, each coefficient in Eq. (21) possesses a physical meaning. Indeed, P_{1r} measures the linear dispersion of the wave; P_{1i} represents the increase in disturbances whose spectra are concentrated in the vicinity of the fundamental wave number k_p; Q_{1r} shows how the frequency of the wave is modulated by nonlinear effects and Q_{1i} expresses the saturation of the unstable wave.[35] Figures 4 and 5 display significant variations of each of these coefficients for various values of the linear dissipation coefficient.

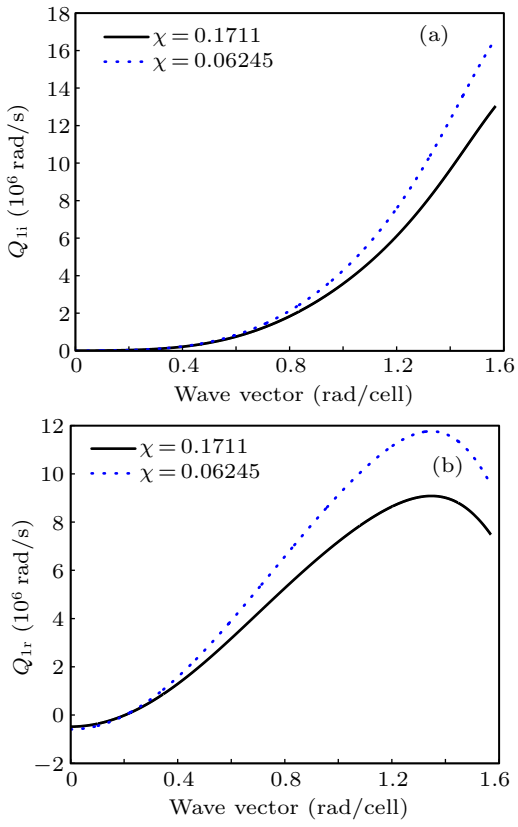


Fig. 5. Effects of the dissipation on the nonlinear coefficient (Q_{1r}, Q_{1i}) versus of the wave number for the line parameters of Fig. 2 and several values of χ.

5.2. Asymptotic behavior of modulated waves

The modulational instability (MI) phenomenon is a basic process that informs on the asymptotic behavior of a plane wave during its evolution in a physical system.[20,24] Also well-known as self-modulation, the MI phenomenon is exploited to classify qualitative dynamics of modulated waves and may initialize the formation of stable entities such as bright solitons.[36,37] In 2001, Pelap *et al.*[24] studied analytically and numerically this phenomenon in a lossless bi-inductance transmission lines and found that, in the HF mode, the occurrence of this phenomenon in the network strongly is linked to the sign of the pseudo product $P_{1r}Q_{1r}+P_{1i}Q_{1i}$. Owing to the literature, it is well known that a plane wave introduced in the system described by an amplitude equation of CGL-type is unstable under modulation if $P_{1r}Q_{1r}+P_{1i}Q_{1i}>0$ and stable otherwise.[14,38,39] This allows us to check the behavior of this pseudo product in terms of the wave number of the carrier for the dissipative NLBTL described by Eq. (21) (see Fig. 6). This curve shows that $P_{1r}Q_{1r}+P_{1i}Q_{1i}$ changes its sign for particular values of the wave number k_p chosen in the first Brillouin zone ($0\le k_p\le \pi/2$) and for the linear dissipation factor taken as $\chi=0.1711$.

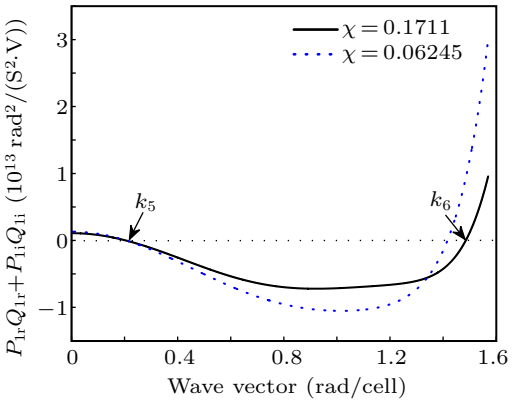


Fig. 6. High frequency evolution of the pseudo product $P_{1r}Q_{1r}+P_{1i}Q_{1i}$ versus the wave vector k_p for the line parameters of Fig. 2. It appears that $P_{1r}Q_{1r}+P_{1i}Q_{1i}$ changes its sign for particular values of the wave vector and given values of the linear dissipative coefficient χ. For the parameters $\chi=0.1711$, the different critical wave numbers of the carrier are respectively $k_5=0.2042$ rad·cell^{-1} and $k_6=1.486$ rad·cell^{-1}.

Figure 6 displays that the growth of the dissipative coefficient modifies the values of the critical wave numbers of the carrier but does not change the number of stability frequency domains. The curves establish the existence of three regions concerning the modulation of the plane wave in the lattice and possible soliton solutions of the amplitude Eq. (21).[38,39] Related details are given below.

In region I, the wave number of the carrier k_p belongs to $0\le k_p\le k_1$ with the critical wave number $k_5=0.2042$ rad/cell. Since $P_{1r}Q_{1r}+P_{1i}Q_{1i}>0$ in this region, a plane wave moving in the lattice with a frequency f chosen in the range $[f_{H\max}, f_5]$ with $f_5=3156$ kHz, $f_{H\max}=3174$ kHz is unstable under modulation and, Eq. (21) possesses an envelope soliton solution.[38,39] The quantity $f_{H\max}$ defines the upper cut-off frequency of the HF mode of transmission.

In region Ⅱ, the carrier wave number k_p and frequency f are taken, respectively, in the ranges $k_5\le k_p\le k_6$ and $f\in[f_5, f_6]$ with the critical wave number of the carrier wave $k_6=1.486$ rad·cell^{-1} and the corresponding critical frequency $f_6=2598$ kHz. Within this region, the pseudo product $P_{1r}Q_{1r}+P_{1i}Q_{1i}$ is negative and any plane wave introduced in the line is stable under modulation. Therefore, the amplitude wave Eq. (21) admits a dark soliton solution.[38,39]

In region Ⅲ, we have $k_6 \leq k_p \leq \pi/2$ that corresponds to the frequency domain $f \in [f_6,\ f_{Hmin}]$ with the low cut-off frequency of the HF mode $f_{Hmin} = 2587$ kHz. Here, the pseudo product $P_{1r}Q_{1r} + P_{1i}Q_{1i}$ is always positive and a plane wave travelling in the line is modulationally unstable. It appears from the results established in Refs. [38,39] that equation (21) admits an envelope soliton solution.

Hereafter, we recapitulate these results on the dispersion curve of Fig. 7. These curves exhibit three regions of modulational phenomenon depending on the sign of $P_{1r}Q_{1r} + P_{1i}Q_{1i}$ instead of one frequency domain as established for the lossless model.[26] The asymptotic behavior of plane waves and the solitary waves expected in each frequency domain are stressed. In the next section, we will carry out numerical search of the analytical results previously established.

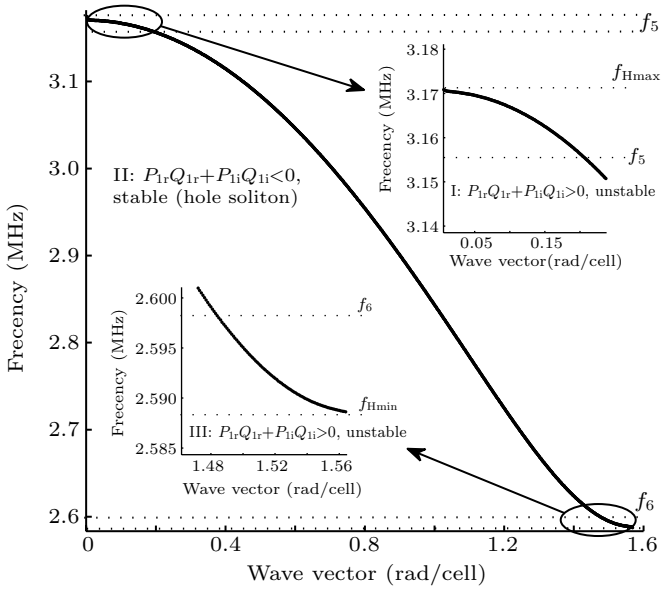


Fig. 7. Dispersion curve with a frequency band divided into three domains dealing with the sign of the pseudo product $P_{1r}Q_{1r} + P_{1i}Q_{1i}$ and defining the stability of the system. The critical frequencies of the carrier are $f_5 = 3156$ kHz, and $f_6 = 2598$ kHz. Tatsinkou *et al.* established the existence of only one domain of frequency in the HF mode of a lossless bi-inductance model.[26]

6. Implementation of the system and numerical simulations

This section deals with the numerical simulations of the dynamics of excitations in the dissipative NLBTL. Here, we do not use the fourth-order Runge–Kutta algorithm to integrate circuit equations as the usual case. The entire network is implemented and simulated by means of the professional LTspice software that uses realistic components for the circuit simulations. In 2015, Pelap *et al.*[37] carried out the similar experiment that exhibits very good results on the 1D mono-inductance nonlinear transmission line using Multisim environments. Hereafter, we introduce some brief details on each part of our system for its better understanding before presenting the results of our findings.

6.1. General concept of the programmable electronic generator

Nowadays it is possible to design generators capable of generating complex signals such as envelope or dark solitons.[40–43] Those generators are exploited in various domains such as nonlinear optics[44–47] and NLTLs.[37,48–50] Therefore, it remains of interest to improve existing generators. Nevertheless, such generators are not essay access. The simplest solution approach should be based on a source directly generating complex signals (bright and dark solitons for example). Unfortunately and to the best of our knowledge, no work has been performed in this direction.

In this subsection, we design a complex generator capable of producing envelope and dark solitons at its output from simplest electronic sources. To reach this aim, we remind that most circuits require an input signal whose amplitude varies over time. This signal may be a true bipolar ac signal or it may vary over a range of dc offset voltages, either positive or negative. It may also be a sine wave or other analogue function, a digital pulse, a binary pattern or a purely arbitrary wave shape. Then, the approach developed uses the contribution of several basic sources for producing the complex output signals (Fig. 8). The choice of such basic sources is motivated by the fact that sine and AM sources can produce signals with frequencies above megahertz (MHz) as a function of each source frequency with the resolution of microHertz (μHz) or even better (e.g., AD9914[51]). We are also encouraged by the possibility to adjust the frequency of the output signal by playing on the frequencies of each source simultaneously.

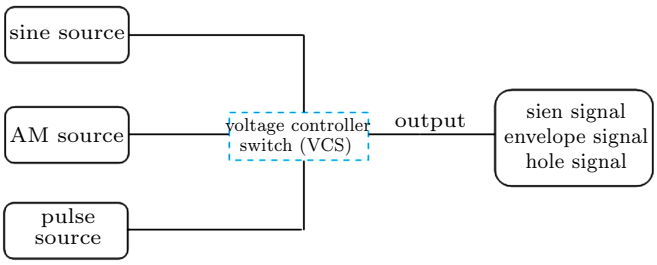


Fig. 8. Block diagram of the proposed PEG.

Then, we implement the PEG of Fig. 8 in the LT-Spice software environment as depicted in Fig. 9. This chart represents the analogue simulator of the PEG consisting of three input sources (two sinusoidal, one pulse) and three output sources (sinusoidal, bright soliton, dark soliton). The sinusoidal source V1 sends an amplitude modulated signal through A1 while the source V3 delivers a signal which is combined with the one supplied by A1 helping to construct the frequency of the carrier wave. The pulse generator V2 intervenes in the management of the voltage controlled switches S1, S2 and S3 allowing the PEG to produce different signals in various outputs depending on the needs of the user.

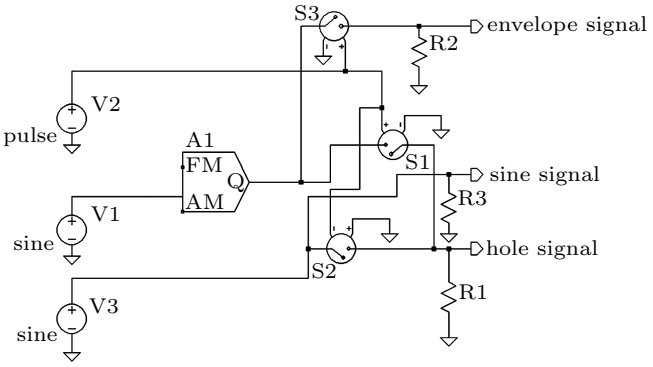


Fig. 9. LT-Spice diagram of our PEG.

6.2. Description of the simulation device

The entire system for simulating the transmission of diverse excitations in the dissipative NLBTL is displayed in Fig. 10. The PEG of Fig. 9 is utilized to generate waves with desired characteristics used as input signals for the dissipative NLBTL. The behavior of these signals will be observed during their propagation in the network having 58 identical unit cells made each of two diodes BB112 biased by a dc voltage $V_p = 1,5$ V through a resistance $r_d = 5$ MΩ. The linear capacitors C_c and C_{osc} are used to block the dc biased current but have no effect on the frequencies range. The linear resistor R_f is also introduced to protect the programmable generator (SRC module). The linear inductors $L_1 = 28$ μH and $L_2 = 14$ μH possess associated resistances r_1 and r_2, respectively. The conductance of the differential diode is linked to the resistance r_p. The input waves are created in the PEG and after their propagation in the network, their waveforms are observed and stored in the numerical oscilloscope XSC1. The frequencies of these waves are chosen in the different regions of the HF mode of transmission summarized in Fig. 7.

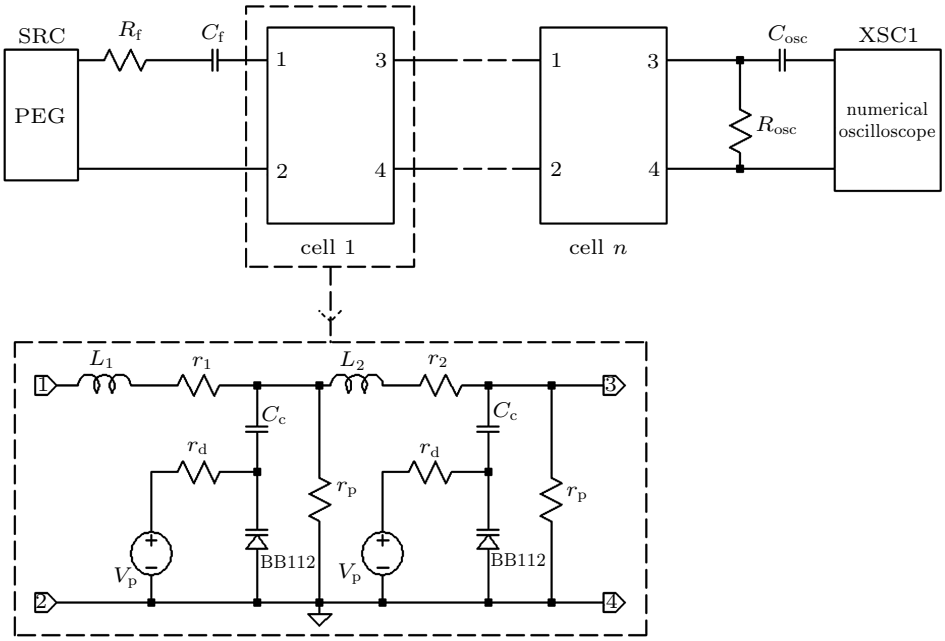


Fig. 10. Representation of the entire simulation system.

6.3. Numerical results

6.3.1. Impact of the dissipation

First, the effect of the dissipation on the dynamics of a plane wave travelling in the system is observed. The curves of Fig. 11 show the attenuation of the signal amplitude in cells 31 and 51 compared to that of the initial wave in cell 1. We could note a diminution of about 36% of the signal energy in cell 31 and 50.4 % in cell 51.

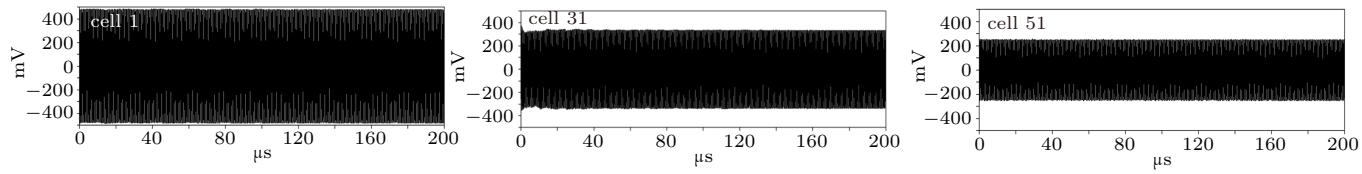


Fig. 11. Dissipation effects on the dynamics of a plane wave in the network for the carrier frequency $f_p = 2802$ kHz and the carrier amplitude $A_p = 500$ mV.

6.3.2. Observation of the modulational phenomenon

Here, we carry out numerical investigations of the MI phenomenon in the dissipative NLBTL for plane wave frequency belonging to the HF mode of transmission. Input plane wave signals generated by the PEG with desired characteristics are

directly injected in the first cell of the line. Cells 1, 20, 31 and 51 are considered for the observation of their asymptotic behavior in the lattice. Figures 12–14 exhibit the results obtained for the carrier wave frequencies $f_p = 3157.2$ kHz, $f_p = 2762$ kHz, $f_p = 2595$ kHz chosen, respectively, in regions I, II and III.

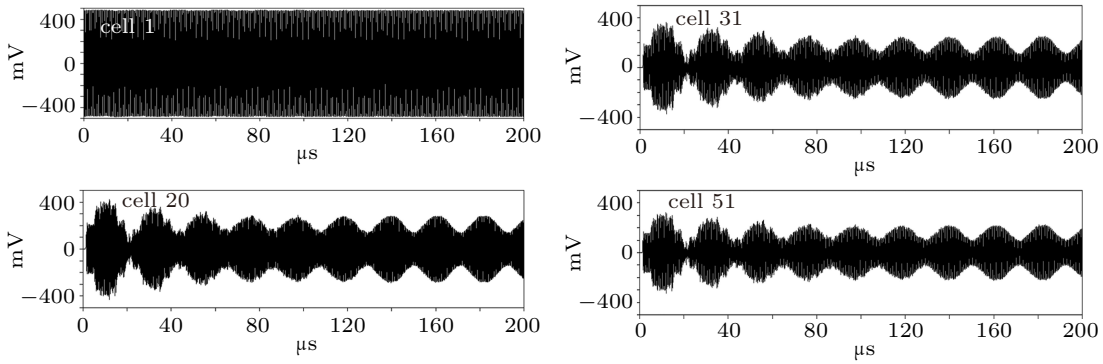


Fig. 12. Temporal evolution of the signal voltage showing the MI of the signal with the carrier frequency $f_p = 3157.2$ kHz chosen in region I of the dispersion curve. We could remark the attenuation of the signal amplitude during its propagation in the system due to the dissipation phenomenon.

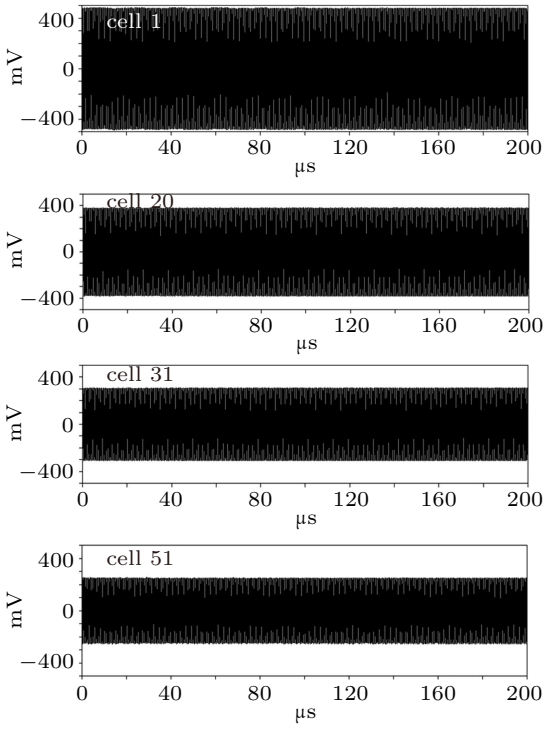


Fig. 13. Temporal evolution of the signal voltage exhibiting the modulational stability (MS) of the signal with the carrier frequency ($f_p = 2762$ kHz) belonging to region II of the dispersive curve. One could observe the diminution of the signal amplitude during its progression dealing with the dissipative character of the network.

It appears from the graphs of Fig. 13 that after a slide adaptation to the line, the signal voltage moves in the NLBTL without modulation. On the other hand, Figs. 12 and 14 show signal voltages that are unstable under modulation during their propagation in the network. Furthermore, these curves (Figs. 12–14) demonstrate that the dissipation phenomenon induces the attenuation of the signal amplitude during the MI phenomenon. These results are in good agreement with our analytical predictions. We could also observe that in the vicinity of the HF lower gap zone, the plane wave loses its memory and exhibits arbitrary behavior (Fig. 15). This last result confirms the fact that the dynamics of waves in the gap zone are governed by other laws.[23]

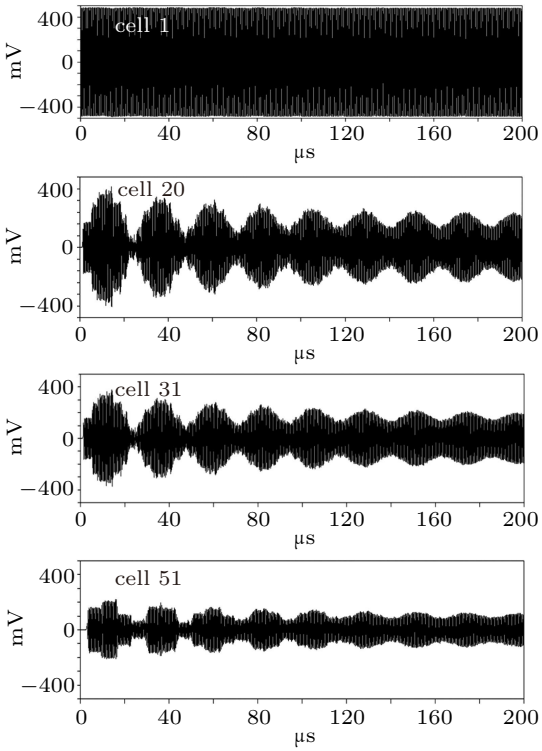


Fig. 14. Modulational instability of the carrier wave with amplitude $A_p = 500$ mV and frequency $f_p = 2595$ kHz chosen in region III of the dispersive curve. We could note the signal attenuation during its motion in the system due to the dissipation: about 24% in cell 20, 44% in cell 31 and around 78% in cell 51 compared to the initial wave.

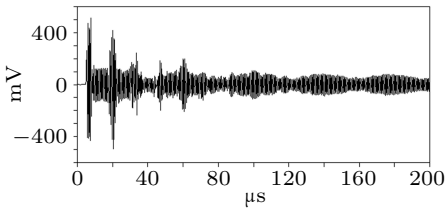


Fig. 15. Numerical observation in cell 31 of the signal voltage of amplitude $A_p = 500$ mV and frequency $f_p = 2347$ kHz belonging to the HF lower gap zone of the dispersive curve.

6.3.3. Propagation of solitary waves in the NLBTL

In this subsection, we investigate the propagation of solitary waves in the dissipative nonlinear bi-inductance transmission of Fig. 1. To achieve this aim, the PEG is adjusted in order to deliver as output signals, an envelope soliton with the characteristics $A_p = 500$ mV, $f_p = 2595$ kHz or $f_p = 3157$ kHz, $f_m = 8.75$ kHz and $m = 1$[27,37] or a dark soliton with the parameters $A_p = 500$ mV, $f_m = 8,75$ kHz, $m = 0.66$ and $f_p = 2762$ kHz.[27,37] In these quantities, A_p defines the amplitude, f_p stands for the carrier frequency, f_m represents the modulation frequency and m designates the modulation index. These output signal voltages are used as input signal for the dissipative NLBTL. Each carrier frequency is chosen in one of the three regions I, II, III of the dispersive curve in Fig. 7 according to the phenomenon to be observed. Cells 1, 16, 32 and 41 are arbitrarily selected to observe the behaviors of the input signal voltages in the network.

Figures 16 and 18 allow observing the propagation of bright soliton waves in the line, respectively, for the carrier frequencies $f_p = 3147$ kHz and $f_p = 2595$ kHz, while Fig. 17 exhibits the motion of the dark soliton wave in the network for $f_p = 2762$ kHz. It appears from these plots (Figs. 16–18) that the solitary waves evolve in the network with an attenuation of their amplitudes, probably due to the presence of the dissipation introduced by the resistances of the inductors and the conductance of the differential capacitor.

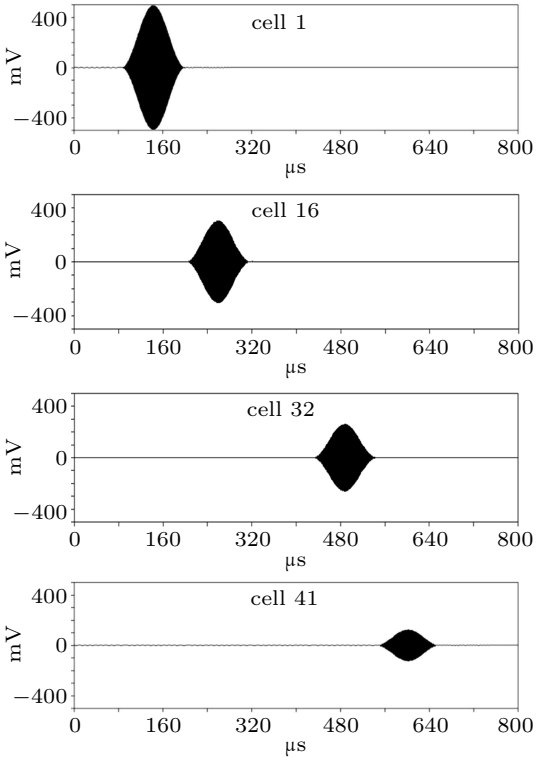


Fig. 16. Propagation of the envelope soliton in the network for the input signal parameters $f_p = 3157$ kHz, $m = 1$, $f_m = 8.75$ kHz and $A = 500$ mV (in cell 1).

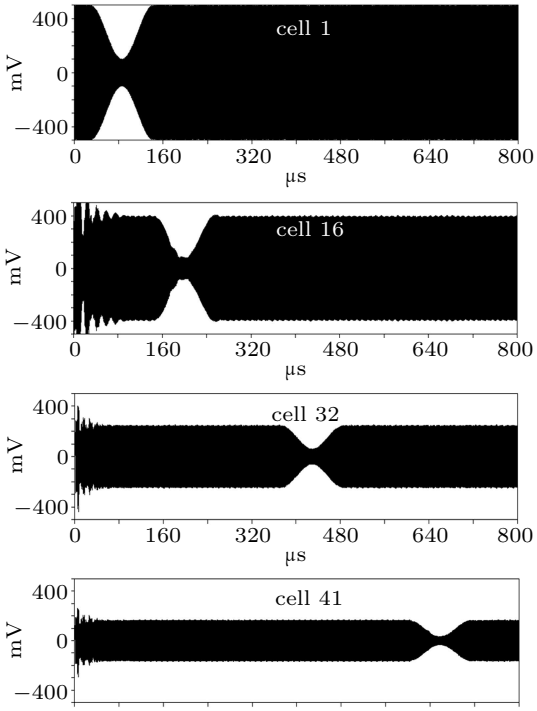


Fig. 17. Transmission of the hole soliton with the characteristics $A = 500$ mV, $f_p = 2762$ kHz, $m = 0.66$ and $f_m = 8.75$ kHz throughout the network of Fig. 1. This signal is generated by the PEG.

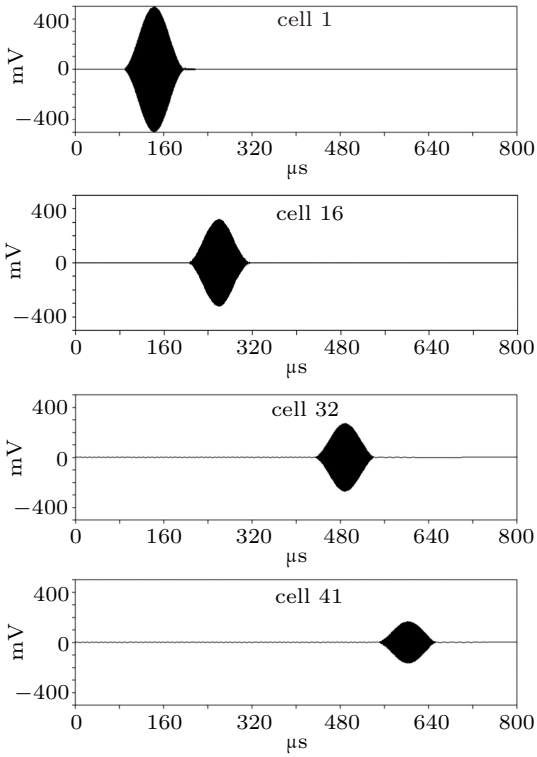


Fig. 18. Propagation of the envelope soliton in the network for the input signal parameters $f_p = 2595$ kHz, $m = 1$, $f_m = 8.75$ kHz and $A = 500$ mV (in cell 1).

7. Discussion and conclusion

In summary, we have theoretically investigated the behavior of the modulated waves in the dissipative NLBTL which is an electrical equivalent of a dissipative nonlinear diatomic chain submitted to cubic interactions in which transversal os-

cillations are neglected. In the linear limit, we show that the network upholds two modes of propagation and made deepness search in the HF mode. We have also shown that the dissipative effects increase with the frequency of the carrier wave. In the continuum limit, we establish that the propagation of HF modulated waves in the dissipative NLBTL is governed by the CGL equation instead of the KdV equation as previously documented. During the study of the asymptotic behavior of a plane wave voltage moving in the dissipative line, there appear three frequency domains of the modulational phenomenon instead of one as obtained earlier[26] for the HF mode of the lossless NLBTL. On the other hand, we propose a design of a complex generator capable of producing envelope and dark solitons at its output from simplest electronic sources. Moreover, these output signal voltages with desired characteristics are utilized as initial conditions to observe some physical phenomena such as wave dissipation, MI phenomenon, envelope and hole propagation in the different frequency domains of the dissipative NLBTL. In all these numerical simulations, we note the attenuation of the signal voltage amplitude during its displacement surely due to the dissipative character of the network. Finally, our established numerical results are in good agreement with the analytical predictions. Furthermore, based on the stability of its outputs, the PEG proposed here could be used for pedagogic and research requirements.

Appendix A: Parameters of Eq. (13)

$$
\begin{aligned}
A &= Y_{12}(\sigma-1)-\mu_{r2}\gamma_{\rm rp},\\
B &= \sigma(b_1Y_{12}-2Y_1),\\
C &= \sigma\left(\frac{b_2}{2}Y_{12}-2b_1Y_1+2Y_1\right),\\
D &= \sigma\left(\frac{b_3}{6}Y_{12}-b_2Y_1+2b_1Y_1-\frac{4}{3}Y_1\right),\\
E &= \sigma\left(\frac{b_4}{24}Y_{12}-\frac{b_3}{3}Y_1+b_2Y_1-\frac{4}{3}b_1Y_1+\frac{2}{3}Y_1\right),\\
F &= \sigma\left(\frac{b_5}{120}Y_{12}-\frac{b_4}{12}Y_1+\frac{b_3}{3}Y_1-\frac{2}{3}b_2Y_1+\frac{2}{3}b_1Y_1-\frac{4}{15}Y_1\right),\\
G &= \sigma\left(\frac{b_5}{120}Y_{12}-\frac{b_4}{12}Y_1+\frac{b_3}{3}Y_1-\frac{2}{3}b_2Y_1+\frac{2}{3}b_1Y_1-\frac{4}{15}Y_1\right),\\
A' &= -Y_{12}\frac{(\sigma-1)}{\sigma}-\mu_{r1}\gamma_{\rm rp},\\
B' &= -Ab_1-b_1Y_{12}+\frac{2Y_1}{\sigma}-\mu_{r1}\gamma_{\rm rp}b_1,\\
C' &= -Bb_1-A\frac{b_2}{2}-\frac{b_2}{2}Y_{12}+\frac{2Y_1}{\sigma}-\mu_{r1}\gamma_{\rm rp}\frac{b_2}{2},\\
D' &= -Cb_1-B\frac{b_2}{2}-A\frac{b_3}{6}-\frac{b_3}{6}Y_{12}+\frac{4}{3}Y_1-\frac{b_3}{6}\mu_{r1}\gamma_{\rm rp},\\
E' &= -Db_1-C\frac{b_2}{2}-B\frac{b_3}{6}-A\frac{b_4}{24}\\
&\quad -\frac{b_4}{24}Y_{12}+\frac{2}{3\sigma}Y_1-\frac{b_4}{24}\mu_{r1}\gamma_{\rm rp},\\
F' &= -Eb_1-D\frac{b_2}{2}-C\frac{b_3}{3}-B\frac{b_4}{24}-A\frac{b_5}{120}\\
&\quad -\frac{b_5}{120}Y_{12}+\frac{4}{15\sigma}Y_1-\frac{b_5}{120}\mu_{r1}\gamma_{\rm rp},\\
G' &= -Fb_1-E\frac{b_2}{2}-D\frac{b_3}{6}-C\frac{b_4}{24}-B\frac{b_5}{120}-A\frac{b_6}{720}\\
&\quad -\frac{b_6}{720}Y_{12}+\frac{4}{45\sigma}Y_1-\frac{b_6}{720}\mu_{r1}\gamma_{\rm rp}.
\end{aligned}
$$

References

[1] Alejandro B A, Gadi F and Boaz I 2004 *Physica D* **189** 277
[2] Alidou M, Jiotsa A K and Kofane T C 2006 *Chaos Solitons and Fractals* **27** 914
[3] Nath R, Pedri P and Santos L 2008 *Phys. Rev. Lett.* **101** 210402
[4] Maucher F, Buccoliero D, Skupin S, Grech M, Desyatnikov A S and Krolikowski W 2009 *Opt. Quantum Electron.* **41** 337
[5] Yamgoue S B, Deffo G R, Tala-Tebue E and Pelap F B 2018 *Chin. Phys. B* **27** 126303
[6] Yamgoue S B, Deffo G R, Tala-Tebue E and Pelap F B 2018 *Chin. Phys. B* **27** 096301
[7] Remoissenet M 1999 *Waves Called Solitons* 3rd edn (Berlin: Springer)
[8] Scott A 1999 *Active Nonlinear Waves Propagation in Electronics* (Oxford: Oxford University Press)
[9] Afshari E and Hajimiri A 2005 *IEEE J. Solid State Circuits* **40** 744
[10] Makenne Y L, Kengne R and Pelap F B 2019 *Chaos Solitons and Fractals* **127** 70
[11] Ndzana F Ⅱ and Mohamadou A 2019 *Chaos* **29** 013116
[12] Iqbal S A and Karim Samsul Ariffin Abdul 2020 *Results in Physics* **18** 103309
[13] Pelap F B and Kofane T C 2001 *Phys. Scripta* **64** 410
[14] Descalzi O, Martinez S and Tirapegui E 2001 *Chaos Solitons & Fractals* **12** 2619
[15] Pelap F B and Faye M M 2004 *J. Phys. A: Math. Gen.* **37** 1727
[16] Pelap F B and Faye M M 2007 *J. Phys. Soc. Jpn.* **76** 074602
[17] Kengne E and Vaillancourt R 2009 *Commun. Nonlinear Sci. Numer. Simulat.* **14** 3804
[18] Yemele D, Talla P K and Kofane T C 2003 *J. Phys. D: Appl. Phys.* **36** 1429
[19] Hafez M G, Iqbal S A, Akther S and Uddin M F 2019 *Results in Physics* **15** 102778
[20] Abdoulkary S, Beda T, Doka S Y, Ndzana F Ⅱ, Kavitha L and Mohamadou A 2012 *J. Mod. Phys.* **3** 438
[21] Yamigno S D 2014 *J. Mod. Phys.* **5** 394
[22] Kofane T C, Michaux B and Remoissenet M 1988 *J. Phys. C: Solid State Phys.* **21** 1395
[23] Essimbi B Z, Ambassa L and Kofane T C 1997 *Physica D* **106** 207
[24] Pelap F B, Kofane T C, Flytzanis N and Remoissenet M 2001 *J. Phys. Soc. Jpn.* **70** 2568
[25] Kengne E, Tadmon C and Vaillancourt R 2009 *Chin. J. Phys.* **47** 80
[26] Pelap F B, Tatsinkou I and Fomethe A 2011 *Phys. Scripta* **83** 045009
[27] Ngounou S M and Pelap F B 2020 *Chin. Phys. B* **29** 040502
[28] Farota A K and Faye M M 2013 *Phys. Scripta* **88** 055802
[29] Farota A K, Faye M M, Diop B, Ndiaye D and Niane M T 2018 *Experimental Studies of the Electrical Nonlinear Bimodal Transmission Line* in *Advanced Electronic Circuits* (IntechOpen)
[30] Tchawoua C, Kofane T C and Bokosah A S 1994 *Phys. Rev. B* **50** 4189
[31] Makhankov V G 1978 *Phys. Rep.* **35** 1
[32] Bekki N 1981 *J. Phys. Soc. Jpn.* **50** 659
[33] Lega L, Janiaud B, Jucquois S and Croquette V 1992 *Phys. Rev. A* **45** 5596
[34] Miguel M S 1995 *Phys. Rev. Lett.* **75** 425
[35] Fernandez-Diaz J M, Guinea A and Palacios S L 2002 *IEEE Photon. Technol. Lett.* **14** 807
[36] Zakharov V E and Ostrovsky L A 2009 *Physica D* **238** 540
[37] Pelap F B, Kamga J H, Yamgoue S B, Ngounou S M and Ndecfo J E 2015 *Phys. Rev. E* **91** 022925
[38] Lange C G and Newell A C 1974 *SIAM J. Appl. Math.* **27** 441

[39] Nozaki K and Bekki N 1984 *J. Phys. Soc. Jpn.* **53** 1581
[40] Hirota R and Suzuki K 1970 *J. Phys. Soc. Jpn.* **28** 1366
[41] Saïdou A, Beda T, Doka S Y, Ndzana F Ⅱ, Kavitha L and Mohamadou A 2012 *J. Mod. Phys.* **2012** 438
[42] Ndjoko P B, Bilbault J M, Binczak S and Kofane T C 2012 *Phys. Rev. E* **85** 011916
[43] Motcheyo A B T, Tchawoua C, Siewe Siewe M and Tchameu J D T 2013 *Commun. Nonlin. Sci. Numer. Simulat.* **18** 946
[44] Mollenauer L F, Neubelt M J, Evangelides S G, Gordon J P, Simpson J R and Cohen L G 1990 *Opt. Lett.* **15** 1203
[45] Rodwell M J, Allen S T, Yu R Y, *et al.* 1994 *Proc. IEEE* **82** 1037
[46] Huang X M H, Feng X L, Zorman C A, Mehregany M and Roukes M L 2005 *New J. Phys.* **7** 247
[47] Kivshar Y S and Agrawal G P 2013 *Optical Solitons: From Fibers to Photonic Crystals* (New York: Academic)
[48] Marquie P, Bilbault J M and Remoissenet M 1994 *Phys. Rev. E* **49** 828
[49] Kenmegne F, Yemélé D and Woafo P 2012 *Phys. Rev. E* **85** 56606
[50] Suchenek M and Starecki T 2012 *Rev. Sci. Instrum.* **83** 124704
[51] Analog Devices AD9914, 2020 accessed on September 20, 2020